Multi-pathway all-optical wavelength conversion switching and routing via four- and six-wave mixing in hot rubidium vapour

2014 Laser Phys. 24 035201

(http://iopscience.iop.org/1555-6611/24/3/035201)

IOP Publishing | Astro Ltd
Laser Physics
Laser Phys. **24** (2014) 035201 (5pp)
doi:10.1088/1054-660X/24/3/035201

Multi-pathway all-optical wavelength conversion switching and routing via four- and six-wave mixing in hot rubidium vapour

Gang Wang[1], Hong-Li Chen[1], Yi Qu[2], Jiao Wang[1], Yan Xue[1], Jin-Hui Wu[1], Mu-Yao Liu[1], Yan-Hui Ren[1] and Jin-Yue Gao[1]

[1] College of Physics, Jilin University, Changchun 130012, People's Republic of China
[2] Changchun Institute of Optics, Fine Mechanics and Physics, Chinese Academy of Sciences, Changchun 130033, People's Republic of China

E-mail: xy4610@jlu.edu.cn and jhwu@jlu.edu.cn

Received 5 June 2013, revised 25 December 2013
Accepted for publication 28 December 2013
Published 10 February 2014

Abstract
We report an experimental demonstration of multi-pathway all-optical switching and routing via efficient wavelength conversion in hot rubidium vapour. We apply a coupling field and a control field to drive both ^{87}Rb and ^{85}Rb isotope atoms into either the double-Λ or triple-Λ configuration when a probe field is scanned across the D1 line of the rubidium atom. We find that this driving scheme facilitates the coherent generation of seven wave-mixing signals with different frequencies and polarizations based on four-wave mixing and six-wave mixing interactions. Also, each generated signal can be switched on and off simply by modulating the control field in frequency to optimize or suppress one specific wave-mixing interaction.

Keywords: optical switching and routing, four-wave mixing, quantum interference

(Some figures may appear in colour only in the online journal)

1. Introduction

Nonlinear optical interactions have facilitated a wide range of photonics applications, for example all-optical switching and routing, which plays a key role in high-speed optical communication networks and quantum information systems [1]. In recent decades, many all-optical switching schemes have been proposed in quantum optics, based on electromagnetically induced transparency (EIT) [2–8], stimulated Raman adiabatic passage (STIRAP) [9, 10], electromagnetically induced absorption gratings (EIG) [11], tunable Fano-like interference [12], nonlinear optical multistability [13], and controlled light storage and retrieval [14, 15]. All-optical routing schemes have also been proposed and demonstrated experimentally, based on light storage and controllable retrieval [16, 17] and photonic band gaps driven by standing-wave fields [18]. These all-optical switching and/or routing proposals all rely on laser-induced quantum interference, and therefore exhibit the advantages of high response speed and low switching power as compared to electro-optical switching schemes.

It is obvious that multi-pathway optical switching is more advantageous than one-pathway switching in improving the communication capacity and efficiency in wavelength division multiplexing systems. However, so far most all-optical switching proposals are implemented as turning on or off one light beam by another light beam. In previous work [19], we have demonstrated two-pathway optical switching based on four-wave mixing (FWM) in hot rubidium vapour, in which both ^{87}Rb and ^{85}Rb atoms are driven into a double-Λ configuration so that two FWM signals are generated with different wavelengths. Here we report an experimental demonstration of multi-pathway optical switching and routing based on four-wave mixing and six-wave mixing (SWM) using the double-Λ and triple-Λ configurations in a Ne-buffered hot-rubidium cell. With the applied coupling, control and probe fields, five FWM signals and two SWM signals could be generated in ^{87}Rb and ^{85}Rb atoms. The intensities of the generated signals can be controlled simply by modulating the control field in frequency to implement optical switching

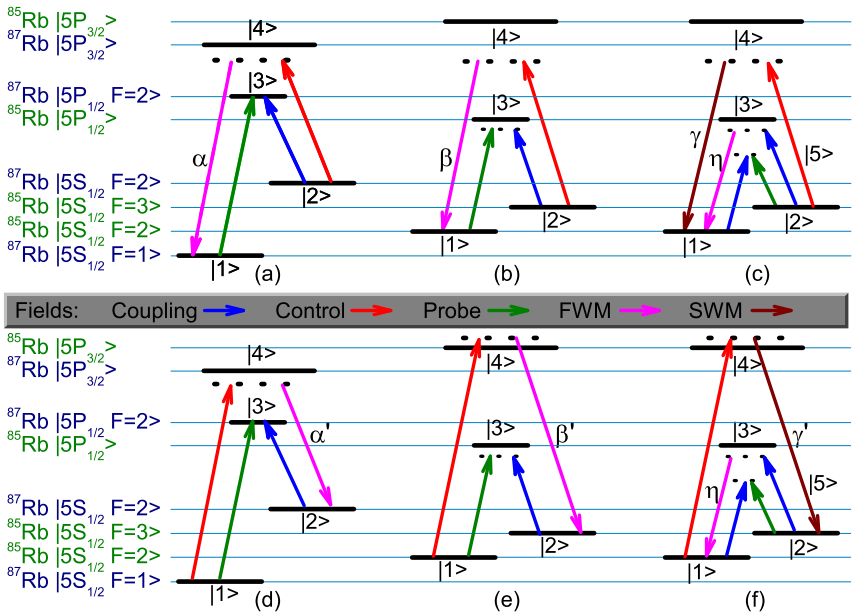

Figure 1. Diagrams of the energy levels and laser excitations in the experiment. The probe, coupling and control fields form four-level double-Λ systems in ^{85}Rb and ^{87}Rb atoms separately and five-level triple-Λ systems in ^{85}Rb atoms to promote the generation of the FWM signals α, α', β, β', η and the SWM signals γ, γ' when the laser fields are applied to the corresponding optical transition. The coupling and control fields drive the corresponding transitions simultaneously in ^{85}Rb and ^{87}Rb atoms, as shown. Also, the coupling field interacts with the virtual level $|5\rangle$ when it is applied to the actual transitions.

and routing, in which three input probe fields with different frequencies are converted controllably to seven output wave-mixing signals with different wavelengths.

2. Energy structures and underlying physics

The atom–light interaction schemes for the proposed all-optical switching and routing are depicted in figure 1. Strong coupling and control fields drive the transitions $|2\rangle \leftrightarrow |3\rangle$ and $|2\rangle \leftrightarrow |4\rangle$ (or $|1\rangle \leftrightarrow |4\rangle$) in both ^{85}Rb and ^{87}Rb atoms respectively due to Doppler broadening in hot atomic vapour. Furthermore, an additional -913 MHz detuning occurs due to the isotope shift between ^{85}Rb and ^{87}Rb atoms when the coupling field is applied to the transition $|2\rangle \leftrightarrow |3\rangle$ of ^{85}Rb atoms, as shown in figures 1(b), (c), (e) and (f). Similarly, the additional detuning of the control field is -1218 MHz for the transition $|2\rangle \leftrightarrow |4\rangle$ (or 2581 MHz for the transition $|1\rangle \leftrightarrow |4\rangle$).

A double-Λ scheme is formed to generate the FWM signals α, α', β, β' at the D2 line ($|5S_{1/2}\rangle \leftrightarrow |5P_{3/2}\rangle$ transition, 780 nm in wavelength) of the rubidium atom when a weak probe field is applied to the transition $|1\rangle \leftrightarrow |3\rangle$, as shown in figures 1(a), (b), (d) and (e). A large control detuning is employed in these cases for efficient FWM due to quantum constructive interference between two opposite FWM processes [20]. The existing large control detuning, in the view of nonlinear optics, would not excessively reduce the nonlinear coefficient $\chi^{(3)}$ associated with the nonlinear optical generation process in the EIT medium and induce a distinct FWM signal, compared with the resonance case for the control field.

Furthermore, the coupling field, as depicted in figures 1(c) and (f), could also drive the transition $|1\rangle \leftrightarrow |3\rangle$ with a large 3.036 GHz (the ^{85}Rb ground-state splitting) additional detuning due to Doppler broadening [21]. For convenience, we denote the virtual level as $|5\rangle$. Therefore, it is instinctive that a FWM signal η would be generated at the D1 line ($|5S_{1/2}\rangle \leftrightarrow |5P_{1/2}\rangle$ transition, 795nm in wavelength) of the rubidium atom on the transition $|1\rangle \leftrightarrow |3\rangle$ when the probe field is applied to the transition $|2\rangle \leftrightarrow |5\rangle$ to form a double-Λ scheme. With the presented control field, the signal generated in the virtual-level FWM process would be reduced due to two-photon absorption [2]. The role of the control field is to disturb the virtual-level FWM process in the double-Λ scheme structured at the D1 line of the rubidium atom, especially when it is in resonance with the corresponding transition $|2\rangle \leftrightarrow |4\rangle$ in figure 1(c) (or $|1\rangle \leftrightarrow |4\rangle$ in figure 1(f)). On the other hand, the applied control field helps to form a triple-Λ scheme and facilitates the generation of a SWM signal γ (or γ') at the D2 line of the rubidium atom on the transition $|1\rangle \leftrightarrow |4\rangle$ in figure 1(c) (or $|2\rangle \leftrightarrow |4\rangle$ in figure 1(f)).

In the considered rubidium isotope ensemble, the FWM and SWM signals generated in eight different schemes are all limited by two necessary conditions. The first condition is that the intensity or efficiency of the FWM (SWM) signal is strictly limited by two-photon resonance between the probe and coupling field [22]. The wave-mixing signals are generated efficiently within the EIT window due to its enhanced nonlinear coefficient $\chi^{(3)}$. The second condition is that the frequency (or detuning) of the control field dominates the enhancement or the reduction of each wave-mixing signal due to the isotope shifts. With the difference among all the considered schemes, one fixed control detuning would help a wave-mixing signal to reach its peak when it synchronously restrains another signal in intensity, or vice versa. In fact, the two conditions enable multi-pathway optical switching and routing implemented as

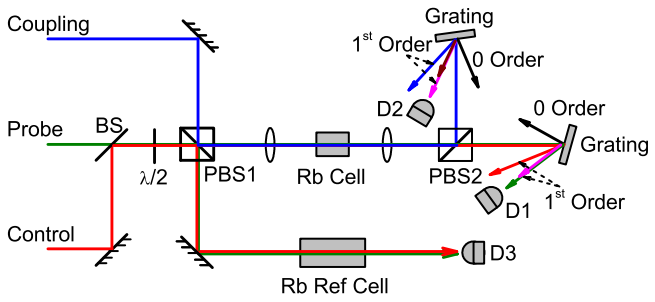

Figure 2. Schematic experimental setup. BS: beam splitter; $\lambda/2$: half-wave plate; PBS: polarization beam splitter; D1, D2 and D3: photodiode.

three input and seven output wavelengths different from each other in the composite ensemble.

3. Experimental setup

The optical switching and routing experiment is performed using a heated, magnetically shielded, 5.0-cm-long, rubidium vapour cell of natural isotopic abundance containing 20 torr of neon buffer gas. The temperature of the cell is heated to ~70 °C. The experimental setup is depicted in figure 2. The frequency of the coupling laser is set to be in resonance with the optical transition connecting the $|5S_{1/2}F = 2\rangle$ ground state to the $|5P_{1/2}F' = 2\rangle$ excited state of the D1 line of the ^{87}Rb atom at 795 nm. The coupling field simultaneously drives the optical transition $|5S_{1/2}F = 3\rangle \leftrightarrow |5P_{1/2}\rangle$ of ^{85}Rb with −913 MHz detuning (because the excited state splitting is only 362 MHz and the Doppler-broadened linewidth is ~500 MHz at room temperature, we may regard the excited states $5P_{1/2}$ as a single energy level). The probe laser is scanned across the D1 line of the rubidium atom and can be set to a frequency in two-photon resonance with the coupling field when it is necessary. The control laser is scanned across the D2 line of the rubidium atom to drive the corresponding transitions of ^{87}Rb and ^{85}Rb (with −1218 or 2581 MHz detuning) atoms (because the total splitting of $5P_{3/2}$ are 496 MHz for ^{87}Rb and 213 MHz for ^{85}Rb, which are smaller than Doppler broadening at 70 °C, we may regard the excited states $5P_{3/2}$ as a single energy level) and can also be set to a frequency to achieve the best on/off switching status. Before entering the cell, the measured powers of the coupling, control and probe laser are 22.4 mW, 4.85 mW and 1.2 mW respectively.

All laser beams are linearly polarized and co-linearly propagate inside the vapour cell with the help of a half-wave plate and a polarization beam splitter (PBS1). The collinear laser beams are focused inside the vapour cell by a lens ($f = 30$ cm) to allow the probe beam to be completely contained in the coupling and control beams so that all probed atoms are coherently prepared. After leaving the vapour cell, the coupling field and the generated FWM (or SWM) signals at 780 nm will be reflected by a polarization beam splitter (PBS2), while the control, probe field and the generated FWM signal at 795 nm will pass through PBS2 due to their perpendicular polarizations relative to the coupling field and the FWM (or SWM) signal at 780 nm. A grating with a groove density of

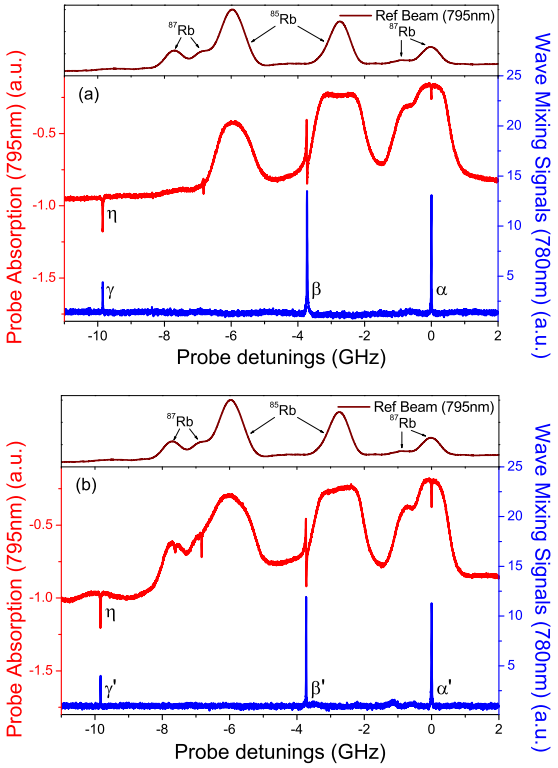

Figure 3. Typical plots of the measured FWM and SWM signals as a function of the probe detunings. In each plot, the absorption spectrum of the D1 line of the rubidium atom as a reference in frequency is shown at the top and the generated FWM and SWM signals spectrum is presented at the bottom. The control field used in (a) (or (b)) drives the transition $|2\rangle \leftrightarrow |4\rangle$ (or $|1\rangle \leftrightarrow |4\rangle$), as shown in figures 1(a)–(c) (or figures 1(d)–(f)) with ~−1.41 GHz (or ~5.92 GHz) detuning. The virtual-level FWM signal η is presented as a downward spine on the left of the probe absorption spectrum (red line) and the other FWM signals α, α', β, β' and SWM signals γ, γ' are generated at 780 nm (blue line). The probe frequencies are scaled by setting the zero probe detuning when the probe field is in resonance with the optical transition $|5S_{1/2}F = 1\rangle \leftrightarrow |5P_{1/2}F' = 2\rangle$ of ^{87}Rb, in which two-photon resonance is formed between the probe and coupling fields in ^{87}Rb.

1200 lines mm^{-1} is used to spatially separate the control field at 780 nm and the probe field, the generated FWM signal at 795 nm. Photodiode D1 monitors the transmission spectrum of the probe beam when it is scanned in frequency. Another grating, the same as the first one, is used to spatially separate the coupling field and the FWM (or SWM) signals at 780 nm. Photodiode D2 is used to detect the generated FWM (or SWM) signals. A small fraction of the probe (or control) beam is reflected by PBS1 and then passes through a 7.5 cm-long rubidium vapour cell of natural isotopic abundance to monitor the absorption spectrum at room temperature as a reference signal using photodiode D3.

4. Experimental results and discussions

We first show, in figure 3, a plot of the measured FWM and SWM signals as a function of the probe frequencies across the D1 line of the rubidium atom. With the applied large-detuned (~−1.41 GHz) control field, an enhanced FWM signal α

(blue line in figure 3(a)) is generated within a reduced EIT dip [22] (red line), which corresponds to the energy model in figure 1(a). The FWM signal β is generated via ^{85}Rb atoms corresponding to the configuration in figure 1(b) only when the probe detuning is set to ~ -3.8 GHz. Furthermore, we observe a probe gain peak η (red line) at the ^{85}Rb ground-state splitting of 3 GHz to the red side of the control frequency, which is due to the virtual-level FWM process implemented in the D1 line of ^{85}Rb, as described in the model in figure 1(c). At the same probe frequency ($\sim$9.8 GHz), we can also observe a prominent signal γ (blue line) at 780 nm, which is generated with the benefit of the applied control field and results from a SWM process, as shown in a triple-Λ model including the D1 and D2 lines of ^{85}Rb in figure 1(c). On the other hand, when the control field is tuned to drive the transition $|1\rangle \leftrightarrow |4\rangle$ with $\sim$5.92 GHz detuning, four similar wave-mixing signals α', β', γ', and η are presented in figure 3(b), which correspond to the models in figures 1(d)–(f) respectively.

For a clear and overall insight into the switching status dependence on the control frequencies, we show a plot of each measured FWM and SWM signal in figure 4 as a function of the control detunings, in which two-photon resonance is formed between the probe and coupling fields, respectively, according to the schemes in figure 1. The wave-mixing efficiencies are measured by dividing the intensity of the wave-mixing signals by the off-resonant probe transmission intensity. The experimental data used in the curves in figure 4 are averaged over 512 measurements because of instability in the intensity and frequency of the laser we employed.

Each of the observed FWM signals ($\alpha, \alpha', \beta, \beta'$) in the D2 line of the rubidium atom (including ^{85}Rb and ^{87}Rb), as shown in figures 4(a) and (b), presents a minimum in intensity due to destructive interference for the resonance case [23], when the control field is tuned to be in resonance with the corresponding transition. However, the same signal reaches its peak in intensity on both sides departing from the resonance, due to constructive interference when a large control detuning is employed. This result agrees with previous work [20]. For the FWM signal η generated in the D1 line of ^{85}Rb, as shown in figure 4(d), the role of the control field is to destroy the FWM process, especially in the resonance case, due to two-photon absorption for the ^{85}Rb atom and a minimum in the FWM signal intensity is presented when the control field is tuned to be in resonance with the corresponding transition of ^{85}Rb. Furthermore, the SWM process is decreased by the attenuated FWM signal η in the D1 line of ^{85}Rb and also suffers, as for the FWM process in the D2 line of the rubidium atom, from destructive interference for the resonance case. In the schemes shown in figures 1(c) and (f) for implementing the SWM process, it can be regarded as a combination of a FWM process in the D2 line of the rubidium atom (as depicted in figures 1(b) and (e)) and a FWM process in the D1 line of the rubidium atom (using the actual level $|3\rangle$ and the virtual level $|5\rangle$ in figures 1(c) and (f)). The contribution from the latter FWM process is less than that from the former FWM process [24], so that the profile of the SWM signal as shown in figure 4(c) is similar to that of the FWM signal in the D2 line of the rubidium atom in figure 4(b). We label the

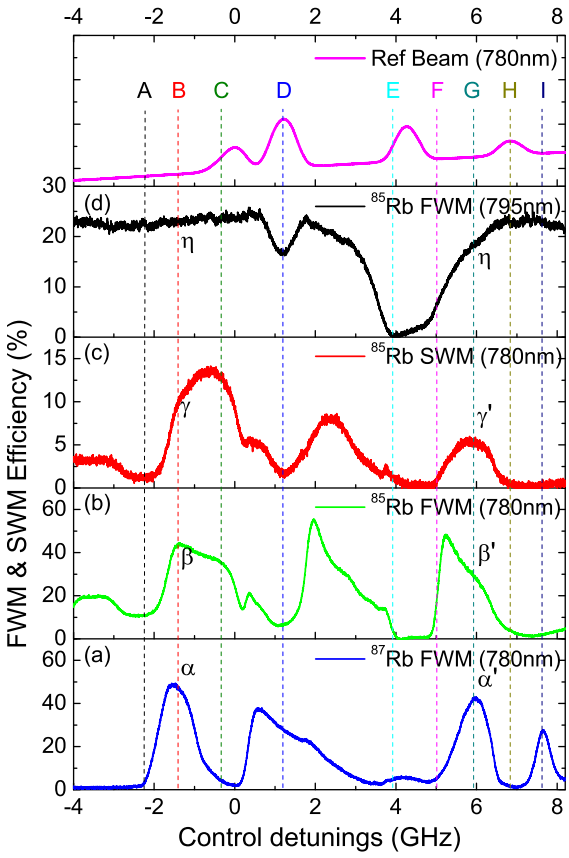

Figure 4. The measured FWM and SWM signal spectra as a function of the control detunings when two-photon resonance is formed between the probe ($\sim$0.0 GHz, $\sim$3.8 GHz, $\sim$9.8 GHz in figure 3) and coupling fields in different schemes, respectively. The emphasized dashed lines denoted from A to I present the possible switching statuses for each wave-mixing signal at different control frequencies. The points B and G correspond to the cases in figures 3(a) and (b), respectively. We set the zero control detuning when the control field is in resonance with the transition $|5S_{1/2}F = 2\rangle \leftrightarrow |5P_{3/2}\rangle$ of ^{87}Rb.

wave-mixing signal spectra with the characters from A to I at several different control detunings to indicate the possible switching statuses. It is clear that excellent output statuses are presented due to the controlled FWM and SWM processes for three fixed probe frequencies.

Considering the difference between the schemes in figures 1(a)–(c) and (d)–(f), the signals generated in the D2 line of the rubidium atom at 780 nm, as depicted in figures 1(a)–(c), are higher (6.8 GHz for ^{87}Rb and 3.0 GHz for ^{85}Rb) in frequency than those in figures 1(d)–(f). We plot the trace of each frequency conversion in figure 5 to present the logical structure of the proposed multi-pathway all-optical switching and routing. The input probe field with $\sim$0.0 GHz detuning is converted separately, via the FWM process of ^{87}Rb, to a FWM signal, according to the scheme shown in figures 1(a) or (d), depending on the control frequencies. A similar branch can also be reproduced for the input probe field b and c (with $\sim$3.8 and $\sim$9.8 GHz detuning respectively), based on the FWM and SWM process of ^{85}Rb. The virtual-level FWM process using the scheme either in figures 1(c) or (f), is only switched on or off by the control field. Therefore, seven controllable

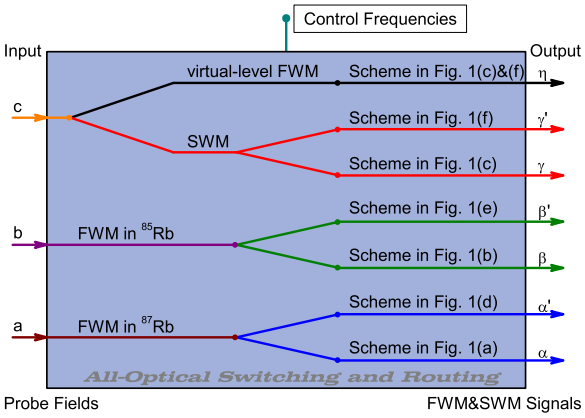

Figure 5. Schematic diagram of the logical structure for the demonstrated optical switching and routing. The input field a, b and c corresponds to a probe field with ∼0.0 GHz, ∼3.8 GHz and ∼9.8 GHz probe detuning respectively, as shown in figure 3.

FWM and SWM signals, distinguished in wavelength, can be observed in the output.

5. Conclusion

In conclusion, we have experimentally demonstrated multi-pathway all-optical wavelength-conversion switching and routing by utilizing four-wave mixing and six-wave mixing processes in a hot-rubidium vapour cell of natural isotopic abundance. Each wavelength conversion in the multi-pathway switching and routing is controlled simply by modulating the control frequency based on the mechanisms of the actual-level wave-mixing signal, with a reduction in intensity due to destructive interference for the resonance case and an enhancement in intensity due to constructive interference for a large control detuning, while the virtual-level wave-mixing signal decreased in intensity due to two-photon absorption for the resonance case. We show that the proposed optical switching and routing is implemented on converting three input probe fields to seven output four-wave mixing or six-wave mixing signals, which are different in wavelength depending on the control frequencies.

Acknowledgments

This work is supported by the National Natural Science Foundation of China (grant nos 11104111, 11174110, 11374125), the National Basic Research Program of China (grant no. 2011CB921603), and the Basic Research Foundation of Jilin University.

References

[1] Miller D A B 2010 *Nature Photon.* **4** 3–5
[2] Harris S E and Yamamoto Y 1998 *Phys. Rev. Lett.* **81** 3611–4
[3] Braje D A, Balic V, Yin G Y and Harris S E 2003 *Phys. Rev.* A **68** 041801(R)
[4] Yan M, Rickey E G and Zhu Y F 2001 *Phys. Rev.* A **64** 041801(R)
[5] Chen Y F, Tsai Z H, Liu Y C and Yu I A 2005 *Opt. Lett.* **30** 3207–9
[6] Zhang J P, Hernandez G and Zhu Y F 2007 *Opt. Lett.* **32** 1317–9
[7] Lin C C, Wu M C, Shiau B W, Chen Y H, Yu I A, Chen Y F and Chen Y C 2012 *Phys. Rev.* A **86** 063836
[8] Lee M J, Chen Y H, Wang I C and Yu I A 2012 *Opt. Express* **20** 11057–63
[9] Ye C Y, Sautenkov V A, Rostovtsev Y V and Scully M O 2003 *Opt. Lett.* **28** 2213–5
[10] Song X L, Wang L, Kang Z H, Lin R Z, Li X, Jiang Y and Gao J Y 2007 *Appl. Phys. Lett.* **91** 071106
[11] Brown A W and Xiao M 2005 *Opt. Lett.* **30** 699–701
[12] Wu J H, Gao J Y, Xu J H, Silvestri L, Artoni M, La Rocca G C and Bassani F 2005 *Phys. Rev. Lett.* **95** 057401
[13] Sheng J, Khadka U and Xiao M 2012 *Phys. Rev. Lett.* **109** 223906
[14] Wang C Y, Chen Y F, Lin S C, Lin W H, Kuan P C and Yu I A 2006 *Opt. Lett.* **31** 2350–2
[15] Lin W H, Liao W T, Wang C Y, Lee Y G and Yu I A 2008 *Phys. Rev.* A **78** 033807
[16] Ham B S 2008 *Phys. Rev.* A **78** 011808(R)
[17] Wang H H, Li A J, Du D M, Fan Y F, Wang L, Kang Z H, Jiang Y, Wu J H and Gao J Y 2008 *Appl. Phys. Lett.* **93** 221112
Wang H H, Fan Y F, Wang R, Du D M, Zhang X J, Kang Z H, Jiang Y, Wu J H and Gao J Y 2009 *Opt. Express* **17** 12197–202
[18] Gao J W, Wu J H, Ba N, Cui C L and Tian X X 2010 *Phys. Rev.* A **81** 013804
[19] Wang G, Xue Y, Wu J H, Liu S S, Jiang Y, Kang Z H and Gao J Y 2009 *Opt. Express* **17** 23332–7
[20] Wang G, Xue Y, Wu J H, Kang Z H, Jiang Y, Liu S S and Gao J Y 2010 *Opt. Lett.* **35** 3778–80
[21] McCormick C F, Boyer V, Arimondo E and Lett P D 2007 *Opt. Lett.* **32** 178–80
Boyer V, McCormick C F, Arimondo E and Lett P D 2007 *Phys. Rev. Lett.* **99** 143601
Camacho R M, Vudyasetu P K and Howell J C 2009 *Nature Photon.* **3** 178–80
[22] Wang G, Cen L, Qu Y, Xue Y, Wu J H and Gao J Y 2011 *Opt. Express* **19** 21614–9
[23] Payne M G and Deng L 2005 *Phys. Rev.* A **65** 063806
[24] Chen Y H, Lee M J, Wang I C, Du S, Chen Y F, Chen Y C and Yu I A 2013 *Phys. Rev. Lett.* **110** 083601